

Diffraction imaging by uniform asymptotic theory and double exponential fitting

Jingtao Zhao^{1,2}, Yanfei Wang^{2*} and Caixia Yu²

¹Research Institute of Petroleum Exploration & Development, PetroChina, Beijing, 100083, P.R. China, and ²Key Laboratory of Petroleum Resources Research, Institute of Geology and Geophysics, Chinese Academy of Sciences, P.O. Box 9825, Beijing, 100029, P.R. China

Received December 2012, revision accepted February 2014

ABSTRACT

Seismic diffracted waves carry valuable information for identifying geological discontinuities. Unfortunately, the diffraction energy is generally too weak, and standard seismic processing is biased to imaging reflection. In this paper, we present a dynamic diffraction imaging method with the aim of enhancing diffraction and increasing the signal-to-noise ratio. The correlation between diffraction amplitudes and their traveltimes generally exists in two forms, with one form based on the Kirchhoff integral formulation, and the other on the uniform asymptotic theory. However, the former will encounter singularities at geometrical shadow boundaries, and the latter requires the computation of a Fresnel integral. Therefore, neither of these methods is appropriate for practical applications. Noting the special form of the Fresnel integral, we propose a least-squares fitting method based on double exponential functions to study the amplitude function of diffracted waves. The simple form of the fitting function has no singularities and can accelerate the calculation of diffraction amplitude weakening coefficients. By considering both the fitting weakening function and the polarity reversal property of the diffracted waves, we modify the conventional Kirchhoff imaging conditions and formulate a diffraction imaging formula. The mechanism of the proposed diffraction imaging procedure is based on the edge diffractor, instead of the idealized point diffractor. The polarity reversal property can eliminate the background of strong reflection and enhance the diffraction by same-phase summation. Moreover, the fitting weakening function of diffraction amplitudes behaves like an inherent window to optimize the diffraction imaging aperture by its decaying trend. Synthetic and field data examples reveal that the proposed diffraction imaging method can meet the requirement of high-resolution imaging, with the edge diffraction fully reinforced and the strong reflection mostly eliminated.

Key words: Uniform asymptotic theory, Exponential fitting, Kirchhoff diffraction, Diffraction amplitude, Diffraction imaging.

1 INTRODUCTION

Early research about diffraction theory was mainly developed in the fields of optics and acoustics (Baker and Copson 1939; Clemmow 1950, 1951; Copson 1950; Morse and Feshbach 1953; Morse and Ingard 1968; Goodman 1968; Longhurst

1973). With the demand of high-resolution imaging in the petroleum industry, interest in seismic imaging gradually moved toward the use of diffracted/scattered waves. The significance of using seismic diffraction to detect small-scale scattering objects such as faults, reflectivity discontinuities and fractures has been emphasized in many publications (Krey 1952; Hagedoorn 1954; Kunz 1960). However, the imaging results of diffraction are generally masked, as the

*E-mail: yfwang@mail.iggcas.ac.cn

diffraction energy is typically one or two orders of magnitude weaker than that of reflection (Reshef and Landa 2009). Therefore, several authors have suggested the separation of diffraction from reflection before seismic diffraction imaging. The main methods of separating diffraction use the kinematic differences in the time migrated domain. In the time domain, the methods include local slant stack (Harlan, Claerbout and Rocca 1984), plane-wave destruction filters (Taner, Fomel and Landa 2006; Fomel, Landa and Taner 2006, 2007) and many other techniques (Bansal and Imhof 2005). In the migrated dip-angle domain (Reshef and Landa 2009; Landa and Fomel 2008), a hybrid Radon transform is adopted for the separation of diffraction (Klokov and Fomel 2012). Based on a coherent summation of diffracted events along appropriate trajectories, discussions by many geophysicists have examined the diffraction imaging methods involving moveout and amplitude corrections (Landa, Shtivelman and Gelchinsky 1987; Kanasevich and Phadke 1988; Landa and Keydar 1998). Similar to the diffraction summation method, the multi-focusing (Berkovitch *et al.* 2009) and common-reflection-surface techniques (Dell and Gajewski 2011; Asgedom, Gelius and Austeng 2011) have been developed to promote the signal-to-noise ratio of diffraction imaging results by supergather stacking. By employing different focusing geometries of the diffraction and reflection, a focusing–defocusing diffraction imaging approach has been presented (Khaidukov, Landa and Moser 2004). Several publications also introduce diffraction enhancing methods by using appropriate weighting functions to modify the Kirchhoff migration algorithm (Kozlov, Barasky and Korolev 2004; Zhang 2004; Moser and Howard 2008; Burg and Verdel 2011).

Stated thus, most of the diffraction imaging methods focus on removing reflections. Moreover, little work has been conducted on enhancing diffraction energy using dynamic characteristics. Diffraction theory can be used to formulate the dynamic characteristics of diffracted waves. The theory mainly includes the Kirchhoff diffraction theory (Troyer 1970, 1977; Hilterman 1970, 1975; Berryhill 1977; Gelchinsky 1982; Deregowski and Brown 1983) and the geometric theory of diffraction (Keller 1962, 1985; Felsen 1984). The Kirchhoff integral formula derived from Green's function is perfect, but its boundary conditions are difficult to satisfy. In the illuminated zone, these boundary conditions require the total wave fields and the corresponding derivatives, respectively, to be equal to those of the reflected waves. In the shadow zone, there are no wave fields. Thus the boundary

conditions of the Kirchhoff theory disobey a well-known theorem of potential theory (Goodman 1968). The geometric theory of diffraction extended from Fermat's principle assumes the diffraction to be a local effect, and that, away from the edges, the diffracted field behaves like diffracted rays (Keller 1962). However, based on the high-frequency hypothesis, the geometric theory of diffraction fails in the shadow-boundary neighbourhoods of reflected/transmitted waves. In these neighbourhoods, the diffracted waves with their amplitudes reaching the highest values show strong potential in terms of noise immunity for diffraction imaging applications. For diffraction problems of the simple geometric models, the geometric theory of diffraction can give exact solutions. However, due to limitations in applications and the complexity in forming solutions for general models, exact solutions are usually not considered in practical applications.

Based on the uniform asymptotic theory (Lewis and Boersma 1969), we provide more insight into the dynamic characteristics of diffracted waves, especially considering their properties of amplitude weakening and polarity reversal. In calculating the diffraction amplitude weakening coefficients, uniform asymptotic theory requires the computation of a Fresnel integral. Because the integration function of the Fresnel integral is in the form of an exponential, we suggest using double exponential functions to simplify the diffraction weakening function. To ensure that the fitting values are close to the true ones, a trust region algorithm is adopted to retrieve the coefficients of the double exponential functions. For removing reflections, we consider the polarity reversal property of diffracted waves. The Huygens–Fresnel principle is involved for clarifications. These principles defines the reflected waves by the constructive interference of elementary diffractions. Moreover, the elementary diffractions on both sides of the stationary points are symmetric. Therefore, if we reverse the polarity of elementary diffractions on one side of the stationary point, reflected waves will be eliminated. For diffracted waves, the situation will be different. When they cross the primary or secondary shadow boundaries, the polarity of diffracted waves will flip (Klem-Musatov and Aizenberg 1980; Klem-Musatov 1994; Klem-Musatov *et al.* 2008). Instead of the attenuation effect of the conventional Kirchhoff imaging method, the polarity reversal in our algorithm will enhance the imaging energy of diffracted waves. Based on these dynamic characteristics of diffracted waves, we propose a dynamic diffraction imaging method that uses the diffraction weakening function and the polarity reversal property.

2 METHODOLOGY

2.1 Uniform asymptotic theory and the dynamic characteristics of diffracted waves

In forward modelling in complex geologic structures, uniform asymptotic theory is a simple qualitative and quantitative method. It has a definite physical meaning and can be used to accurately calculate the wave fields both in geometrical illuminated zones and in shadow zones. In this theory, the weakening function is defined to express the dynamic characteristics of diffracted waves (Landa *et al.* 1987) and has the following form:

$$W(w) = \begin{cases} \exp(-\pi i w^2/2) F(\zeta), \\ \exp(-\pi i w^2/2) [1 - F(\zeta)], \end{cases} \quad (1)$$

where the first and second terms denote respectively the wave fields in shadow zones and those in illuminated zones. The function $F(\zeta)$ represents the Fresnel integral and is given by

$$F(\zeta) = \pi^{-1/2} \exp(-\pi/4) \int_{-\infty}^{\zeta} \exp(i\tau^2) d\tau, \quad (2)$$

where

$$\zeta = (\pi w^2/2)^{1/2} \quad \text{and} \quad w = \left[\frac{2}{\pi} \omega(t_D - t_R) \right]^{1/2}, \quad (3)$$

with t_D and t_R being respectively the traveltimes of diffracted and reflective waves, and ω is the angular frequency.

Equation (1) reveals an interesting phenomenon that the polarities of diffracted waves will reverse when the diffracted waves cross the geometrical shadow boundary. The weakening function $W(w)$ is a complex function whose absolute values represent the amplitude attenuation of diffracted waves. Numerical calculations indicate that energy distributions of the diffracted waves are mainly located in the neighbourhood of the geometrical shadow boundary. In this neighbourhood, the traveltime difference between diffracted waves and the reflected wave at a stationary point is usually several periods of seismic wavelet.

2.2 Exponential least-squares fitting by means of a trust region method

A symptotic theory has been used to investigate the characteristics of diffracted waves for a long time. However, little attention has been paid to adopting them to develop a diffraction imaging method. The reason is that the diffraction amplitude weakening function is in the complex form of Fresnel integration, which makes the numerical calculation difficult

to implement. Therefore, in applying the uniform asymptotic theory to diffraction imaging, a key issue is how to construct a proper weakening function. Observing that the Fresnel integral function is in the exponential form, we consider employing exponential functions for a proper curve fitting. The best-fitting curve to a given set of points is achieved by minimizing the sum of the squares of the offsets of the points from the curve, which allows the offsets to be treated as a continuous differentiable quantity. The general form of an exponential distribution function can be written as

$$f(t) = a \exp(b(t + c)) + d, \quad (4)$$

where the values of the coefficients a , b , c and d may change continuously. The double exponential distribution function has the general form

$$f(t) = (a_1 \exp(b_1(t + c_1)) + d_1) + (a_2 \exp(b_2(t + c_2)) + d_2), \quad (5)$$

where the coefficients a_i , b_i , c_i and d_i for $i = 1, 2$ are to be determined. We consider the weakening function $W(w)$ in the form of equation (5) with c_i and d_i equal to zero, i.e., $f(t) = a_1 \exp(b_1 t) + a_2 \exp(b_2 t) + d$.

Suppose that the theoretical values of f on each point are known, then our fitting criterion is trying to minimize the residual of the computed one and the theoretical one, i.e., minimize

$$J[x] = \|f(x) - \bar{f}\|^2, \quad (6)$$

where \bar{f} denotes the true function value, $x = [a_1, b_1, a_2, b_2]^T$.

Straightforward calculation shows that the gradient of J at x_k ($x_k = [a_1^k, b_1^k, a_2^k, b_2^k]^T$) is

$$g_k := \text{grad}J(x_k) = \begin{bmatrix} \frac{\partial J}{\partial a_1}(a_1^k) \\ \frac{\partial J}{\partial b_1}(b_1^k) \\ \frac{\partial J}{\partial a_2}(a_2^k) \\ \frac{\partial J}{\partial b_2}(b_2^k) \end{bmatrix} \quad (7)$$

and the Hessian of J at x_k is

$$H_k = \nabla^2 J(x_k) = \frac{\partial}{\partial x_k} (\text{grad}J(x_k)). \quad (8)$$

In solving the minimization problem, two approaches are usually considered: line search or trust region. In a line search method, the model function generates a step direction, and a search is done along that direction to find an adequate point (step size) that will lead to convergence. In a trust region method, a generalized sphere in which the model function will be trusted is updated at each step. If the model

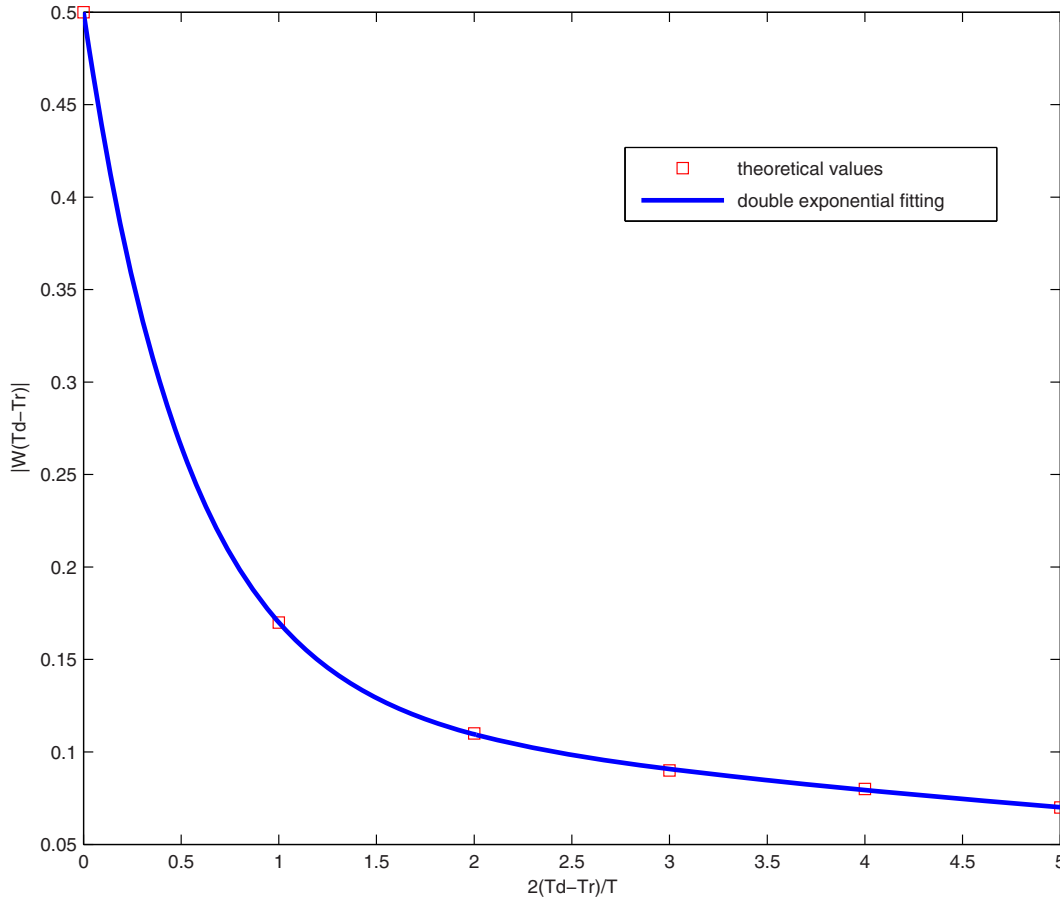


Figure 1 Amplitude weakening curve of diffracted wave by double exponential functions fitting method.

step lies within the sphere, it will be used to update the iterative point; otherwise, an approximate minimum for the model function on the boundary of the trust region is used. Generally, trust region methods are more robust than line search methods. Moreover, for nonlinear least-squares problems (sometimes nonlinear ill-posed problems), the trust region method yields the best convergence results, and the method is a regularization method, which means that it can supply a stable globally convergent solution (Wang and Yuan 2005). Therefore, we consider using the method in the double exponential fitting problem (5).

With the above preparation, a trust region subproblem for the minimization model (6) at the k -th step can be formulated as follows: minimize over \mathbb{R}^4 the function

$$\phi_k(\xi) := (g_k, \xi) + \frac{1}{2}(H_k \xi, \xi), \tag{9}$$

$$\text{subject to } \|\xi\|_{l_2} \leq \Delta_k. \tag{10}$$

Solving the above ball-constrained minimization problem gives ξ_k , and updating $x_{k+1} = x_k + \xi_k$ provides a new iteration.

To solve the trust region subproblem (9)–(10), we introduce the Lagrangian multiplier λ and solve an unconstrained minimization problem:

$$L(\lambda, \xi) = \phi_k(\xi) + \lambda(\Delta_k^2 - \|\xi\|_{l_2}^2) \longrightarrow \min. \tag{11}$$

Straightforward calculation show that the solution satisfies

$$\xi = \xi(\lambda) = -(H_k + \lambda I)^{-1} g_k. \tag{12}$$

Moreover, at the k -th step, the Lagrangian parameter λ can be solved via the nonlinear equation

$$\|\xi_k(\lambda)\|_{l_2} = \Delta_k. \tag{13}$$

In our calculation, λ is solved through Newton’s root-finding method, i.e.,

$$\lambda_{l+1} = \lambda_l - \frac{\Gamma(\lambda_l)}{\Gamma'(\lambda_l)}, \quad l = 0, 1, \dots, \tag{14}$$

Table 1 Fitting results of double exponential form.

ΔT_{dr}	0	1	2	3	4	5
Theoretical	0.5	0.17	0.11	0.09	0.08	0.07
Fitting	0.5	0.1701	0.1095	0.0908	0.0794	0.0701
Error	0	0.0001	0.0005	0.0008	0.0006	0.0001

where $\Gamma(\lambda) = \frac{1}{\|\xi_k(\lambda)\|_{l_1}} - \frac{1}{\Delta_k}$. It can be proved that $\|\xi_k(\lambda)\|_{l_2}$ is a nonmonotonic function of λ and that $\{\lambda_l\}_{l=1,2,\dots}$ is bounded. Details of the implementation are given in Wang and Yuan (2005) and Wang (2007).

Using the trust region method, the optimized coefficients

$$x^* = [a_1^*, b_1^*, a_2^*, b_2^*]^T = [0.3708, -1.8650, 0.1292, -0.1223]^T \quad (15)$$

can be obtained and the fitting curve function of double exponential functions is given as

$$|W(\Delta T_{dr})| = 0.3708e^{-1.865\Delta T_{dr}} + 0.1292e^{-0.1223\Delta T_{dr}}, \quad (16)$$

where ΔT_{dr} represents the traveltime difference between diffracted waves and the reflected wave at a stationary point with a normalization on the half period of the seismic wavelet.

We also considered single exponential least-squares fitting using the above-mentioned trust region method. The results indicate that the values obtained by the double exponential fitting formula (16) agree with the ones from the uniform asymptotic theory to a satisfactory degree. Using our method, the weakening curve of the amplitude of diffracted waves is shown in Fig. 1, where the solid line represents the calculated values, and the rectangles represent the theoretical values. In Table 1, fitting and theoretical values are listed, with the maximum error equal to 0.0008. Comparison of the values shows that our method can provide a good weakening function $W(w)$ for diffraction imaging.

2.3 Imaging conditions of dynamic diffraction imaging method

As is well known, conventional diffraction stack imaging can image all kinds of waves if the traveltimes and weights are calculated accurately (Geoltrain and Brac 1993; Moser 1994; Gray and May 1994; Nichols 1996; Audebert *et al.* 1997; Operto, Xu and Lambaré 2000). The general process of imaging continuous reflectors, justified by the diffraction stack formula, can be physically interpreted as a summation of

weighted amplitudes along Huygens' isochronous surfaces. The weighted factors are reflection-biased and will seriously destroy the energy outside the first Fresnel aperture. Therefore, the principle of conventional imaging is built on idealized point diffractors, whose elementary diffraction responses are tangent to reflection and symmetric about the stationary points. Throughout the process of imaging, elementary diffractions are only mathematical idealizations, destined to construct reflected waves, and cannot be observed independently on a seismic section (Khaidukov *et al.* 2004).

To strengthen diffraction and simultaneously remove reflection, we introduce a diffraction imaging method based on the dynamic characteristics of edge diffractors. Diffraction propagation theory reveals that the edge/tip diffraction will reverse polarity as the diffractors cross the boundary of the primary/secondary geometrical shadow. If the property of polarity reversal is included in the conventional diffraction formulation, reflectors will be completely removed under the condition of symmetrical imaging apertures. According to the uniform asymptotic theory, the weakening function indicates the energy distribution of the diffracted waves beyond the first Fresnel aperture. Moreover, the decaying trend of the weakening function shows that its behaviour is like choosing an inherent aperture for diffraction imaging. By considering the dynamic characteristics of the diffracted waves, we propose a diffraction imaging method that modifies the Kirchhoff imaging formula with a double exponential fitting function and the polarity reversal behaviour.

The conventional Kirchhoff diffraction stack formula can be written as

$$V(x) = \int_{s_{\min}}^{s_{\max}} \int_{r_{\min}}^{r_{\max}} \int_{t_{\min}}^{t_{\max}} \frac{U(t, s, r)}{A(s, x, r)} \delta(t - t_d(s, x, r)) dt dr ds, \quad (17)$$

where $V(x)$ denotes the image at a subsurface point x ; $U(r, s, t)$ represents the recorded seismic data at a receiver point r and source point s ; and $A(s, x, r)$ is the ray-theoretical geometrical spreading term and is positive. The wavefront surface $t_d(s, x, r)$ represents the traveltime of elementary diffraction from source to receivers via an imaging point x .

The dynamic diffraction imaging condition can be written as the following equation:

$$\begin{aligned} V(x) = & \int_{s_{\min}}^{s_{\max}} \int_{r_{\min}}^{r_{\max}} \int_{t_{\min}}^{t_{\max}} \frac{U(r, s, t)}{A(s, x, r) W_+(\Delta T_{dr})} \\ & \times \delta(t - t_d(s, x, r)) dt dr ds \\ & + \int_{s_{\min}}^{s_{\max}} \int_{r_{\max}}^{r_{\min}} \int_{t_{\min}}^{t_{\max}} \frac{U(r, s, t)}{A(s, x, r) W_-(\Delta T_{dr})} \\ & \times \delta(t - t_d(s, x, r)) dt dr ds, \end{aligned} \quad (18)$$

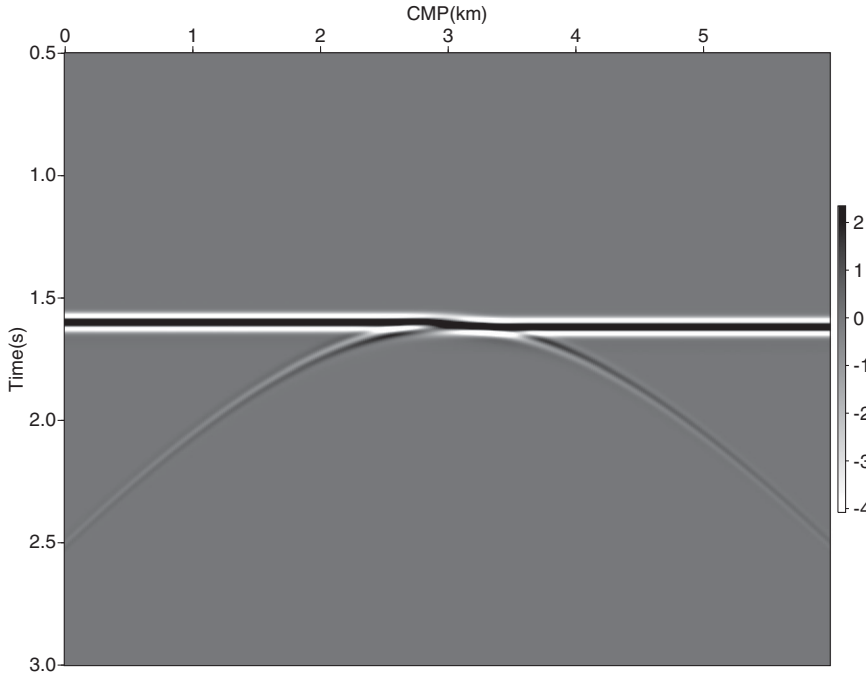


Figure 2 Synthetic zero-offset section of the vertical tiny fault model.

where $W_-(\Delta T_{dr})$ and $W_+(\Delta T_{dr})$ denote the weakening functions in illuminated and shadow zones, respectively. Their absolute values are the same as that of $W(\Delta T_{dr})$, with opposite signs (positive or negative). Here, t_d represents the traveltime of the diffracted wave, r_s is a stationary point position, and r_{\min} and r_{\max} are the left-hand and right-hand positions of the imaging aperture at the stationary point, respectively. These two locations can be derived from the fitting curve, e.g., Fig. 1, by the difference between their traveltimes and that of a stationary ray. If the polarity reversal and symmetrical imaging apertures are considered, then the imaging formula (18) can be revised as follows:

$$V(x) = 2 \int_{s_{\min}}^{s_{\max}} \int_{r_{\min}}^{r_s} \int_{r_{\min}}^{r_{\max}} \frac{U(r, s, t)}{A(s, x, r) |W(\Delta T_{dr})|} \times \delta(t - t_d(s, x, r)) dt dr ds. \quad (19)$$

In the mechanism of conventional Kirchhoff imaging, diffracted waves with polarity reversal across the shadow boundary will destructively interfere with each other. In contrast, the new diffraction imaging formula (19) will strongly enhance them by the same-phase summation and weighted factors of the weakening function. Regarding reflection, polarity reversal will eliminate most of its energy. Based on this distinct imaging principle, we derive a dynamic diffraction imaging method. Note that we use limited symmetric aper-

tures because of the asymmetric survey nature of practical applications. As is well known, calculation of reflection traveltimes at the stationary point is the core issue in diffraction imaging problems. The main techniques include ray tracing (Khaidukov *et al.* 2004; Moser and Howard 2008) and reflector dips scanning (Tygel *et al.* 1993; Marfurt *et al.* 1998; Fomel 2002). To determine the location of a stationary point and obtain the corresponding reflection traveltime, we perform the following procedure: first, traveltimes from source to receivers, via imaging point, are calculated using ray tracing to obtain the whole wavefront surface; then, sliding along the surface, a variable-length window is chosen to scan the strongest energy band, where the centre of window is considered as the stationary point, and the corresponding time is taken as the reflection traveltime.

3 SYNTHETIC DATA EXPERIMENTS

3.1 Vertical tiny fault model

This model is designed to test the focusing ability of our proposed method in dealing with edge diffracted waves. Here a simple geological model consisting of a vertical tiny fault is constructed in a constant-velocity background. The fault is placed at horizontal position of 3000 metres and its vertical displacement is 20 metres. Figure 2 shows a zero-offset

Figure 3 Two interfering edge diffracted waves of the vertical tiny fault model.

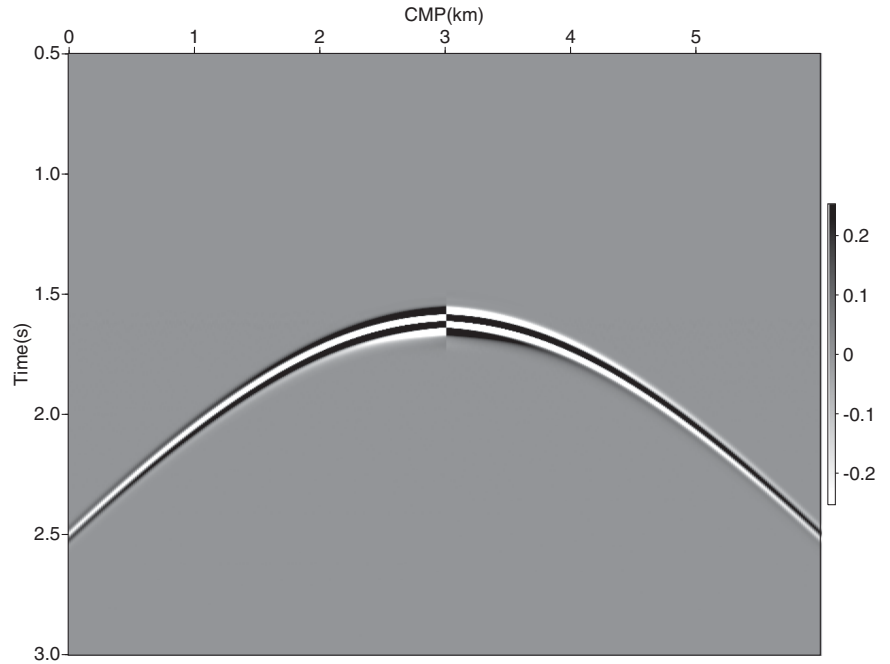
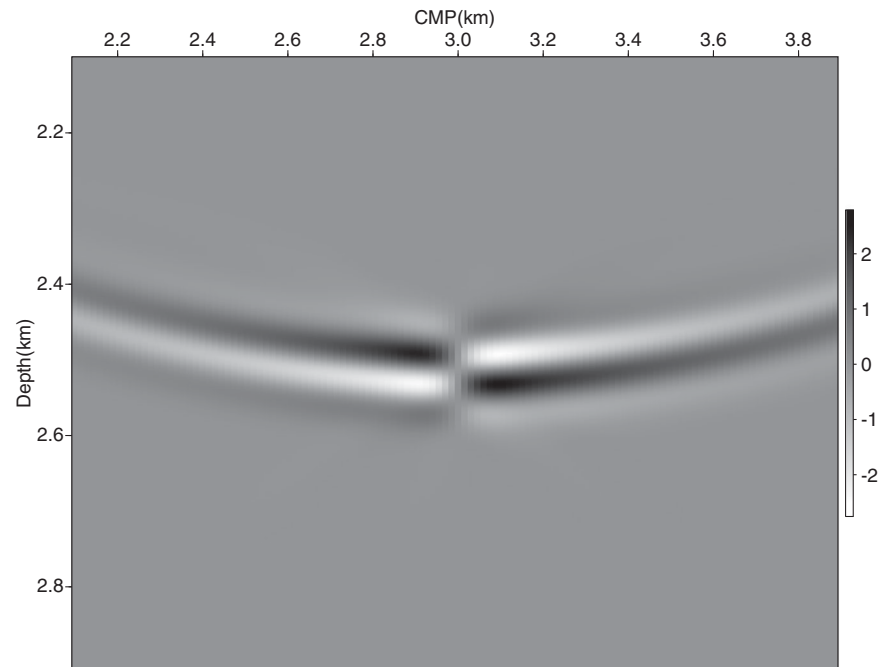


Figure 4 Conventional imaging result of the vertical tiny fault model.



section over this model, synthesized by Kirchhoff modelling with a seismic dominant wavelength of 200 metres. Two types of seismic waves can be distinguished. There are reflected waves from the top and the lower plane interfaces. The right edge of the top reflector and the left edge of the lower reflector create edge diffracted waves. To exclude the effect of

reflected waves on the imaging result, we separate out the diffracted waves, as shown in Fig. 3. The two edge diffracted waves are coupled with each other and identifying them may be difficult. Also, each edge diffraction reverses polarity as it crosses the geometrical shadow boundary. Figure 4 illustrates the result obtained using the conventional Kirchhoff

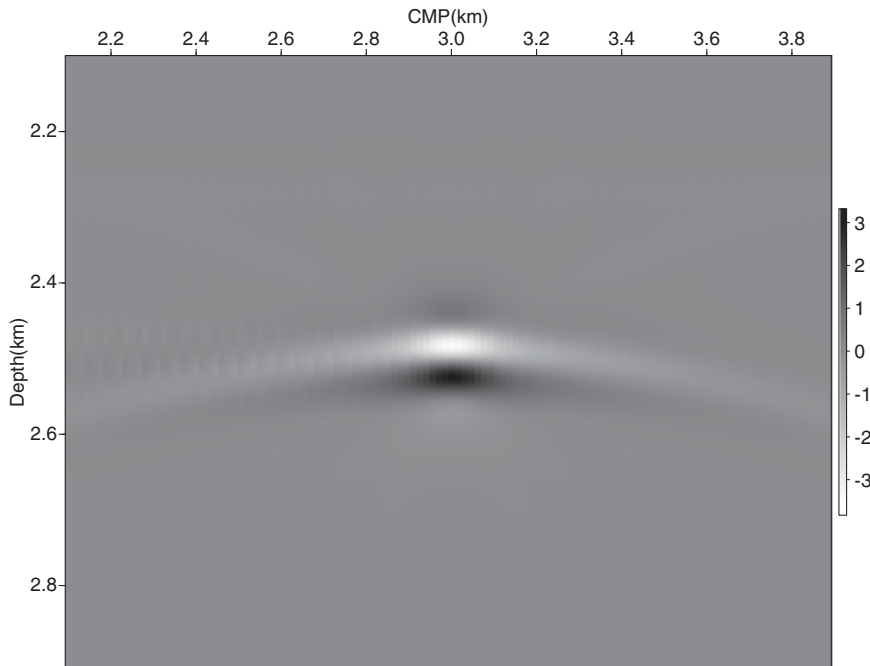


Figure 5 Dynamic diffraction imaging result of the vertical tiny fault model.

migration method. Due to the reversal-phase summation of edge diffractions, edges are not well focused and imaging artefacts appear in the conventional imaging method. The diffraction imaging result obtained using our proposed method is shown in Fig. 5. By the same-phase summation of edge diffractions, two focusing edge points clearly stand out.

By considering both the weakening function and polarity reversal behaviour, the diffraction imaging result in this geological model demonstrates the attractive feature of our proposed method in focusing diffraction. In particular, when dealing with edge diffracted waves, our model's imaging principle offers an obvious advantage.

3.2 Edge and small-scale diffractor model

This model consists of five parallel reflectors and there is a small diffractor in the middle of each reflector. Figure 6 shows the zero-offset synthetic section with diffractions originating from edges and small-scale diffractors. Figure 7 illustrates the imaging result obtained using the conventional imaging method. Parallel dipping reflectors are clearly imaged, but small-scale diffractors are masked in the strong background of reflection. Figure 8 demonstrates the imaging result obtained by our proposed diffraction imaging method. In the diffraction imaging result, both edges and small-scale diffractors are distinguishable and reflectors are removed. Figure 6 indicates that, to maintain continuity of the wave fields, edge diffracted

waves will reverse polarity when crossing the primary shadow boundary. In the shadow zone, the edge diffracted wave keeps the same polarities as the reflected wave, and it does the opposite in the illuminated zone. In imaging diffracted waves, we need to choose $W_+(\Delta T_{dr})$ or $W_-(\Delta T_{dr})$ (see equation (18)) in our diffraction imaging algorithm. In our case, we choose the same sign as that of the left-hand side of the diffracted waves. Figure 8 clearly illustrates that the apparent polarity flips from lower-edge diffractors to top-edge diffractors. The edge and small-scale diffractor model indicates the ability of our diffraction imaging method to remove reflection and to image of edges and diffractors.

3.3 Multi-scale geological model

In this 2D geological model, different scales of vertical faults, edges and diffractors are constructed to test the resolution ability and to demonstrate the imaging characteristics of our proposed dynamic diffraction imaging method. We use Kirchhoff forward modelling to synthesize the zero-offset seismic record, with the seismic dominant wavelength equaling 200 metres. The geological model is shown in Fig. 9. In the upper part of the model, there are five tiny vertical faults whose vertical displacements are respectively λ , $\lambda/4$, $\lambda/8$, $\lambda/16$ and $\lambda/40$. In the middle, there are several horizontal discontinuities whose scales and sequences are the same as those of tiny faults. In the bottom, we buried six diffractors whose

Figure 6 Synthetic zero-offset section of edge and small-scale diffractor model.

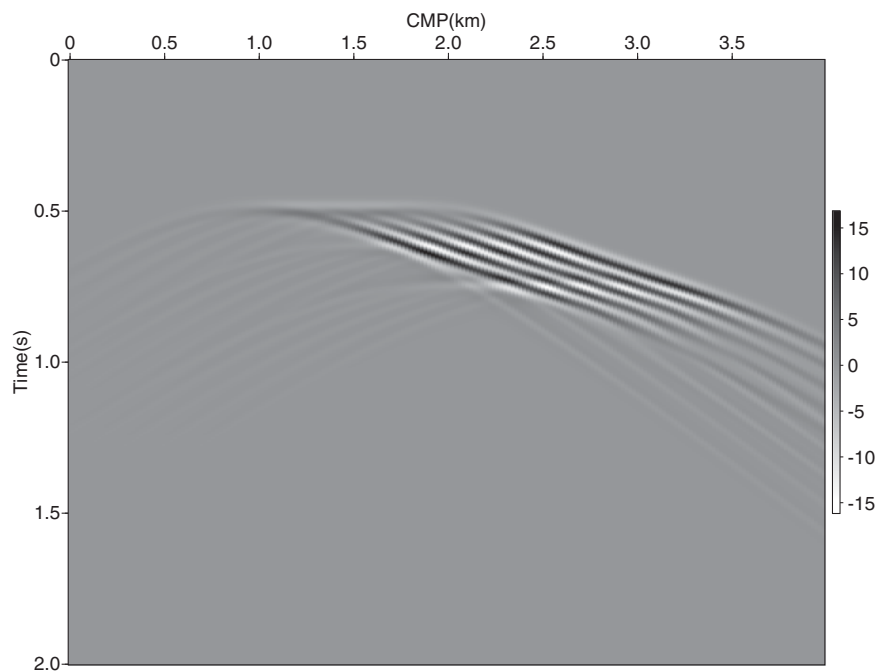
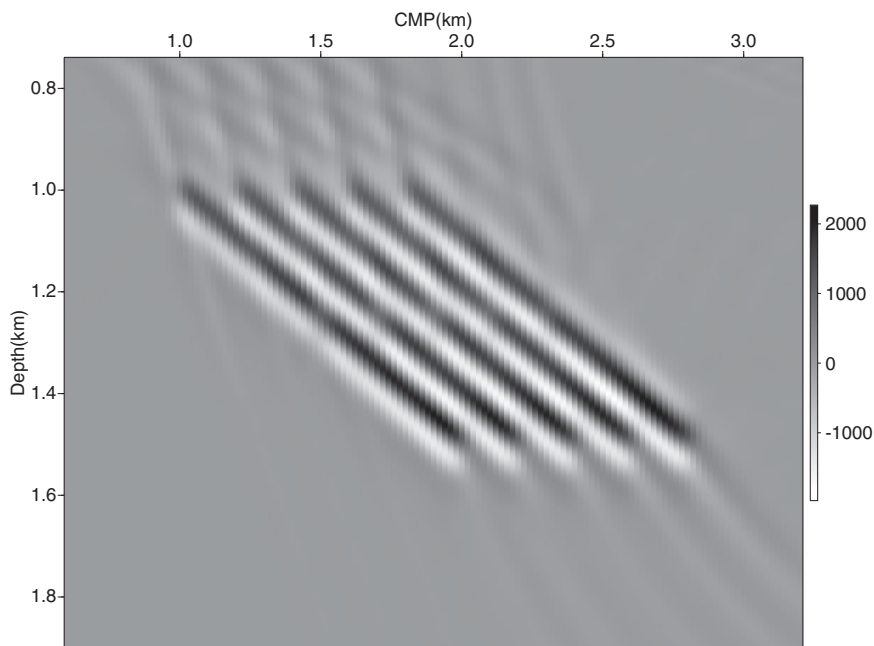


Figure 7 Conventional imaging result of the edge and small-scale diffractor model.



scales are respectively $\lambda/30$, $\lambda/16$, $\lambda/8$, $\lambda/4$, $\lambda/2$ and λ . The synthetic zero-offset record is shown in Fig. 10, where the energy of diffracted waves from small-scale geologies is weak. The imaging result obtained using the conventional imaging method is shown in Fig. 11, where the macro-scale reflectors are clearly imaged. However, it is hard to classify the

small-scale vertical faults. For the horizontal discontinuities, the situation is even worse. Using the proposed diffraction imaging method, we obtain the imaging result shown in Fig. 12. The diffraction imaging result illustrates some obvious phenomena. First, polarity reversal eliminates most of the reflections. Second, for the tiny vertical faults, only up/down

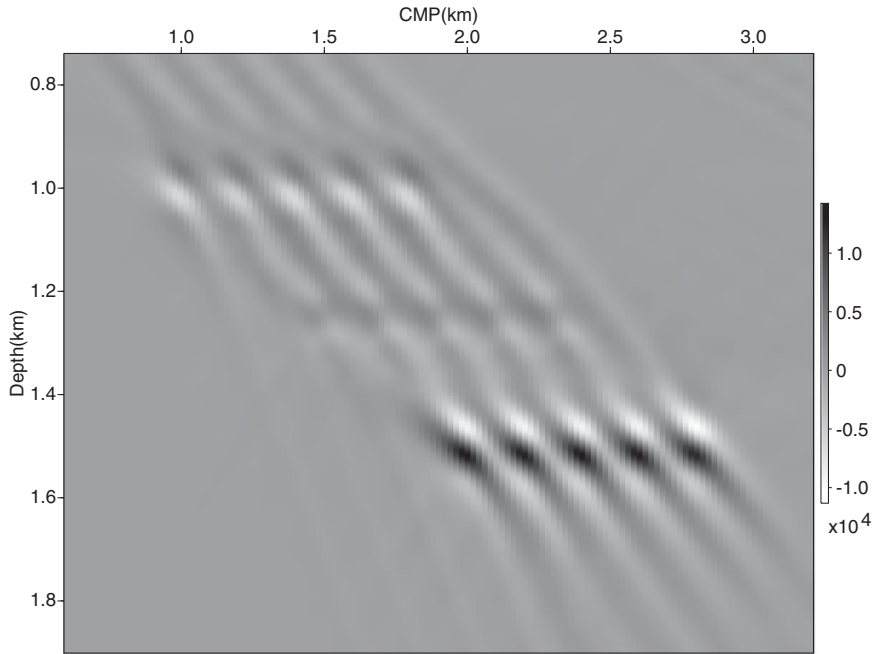


Figure 8 Dynamic diffraction imaging result of the edge and small-scale diffractor model.

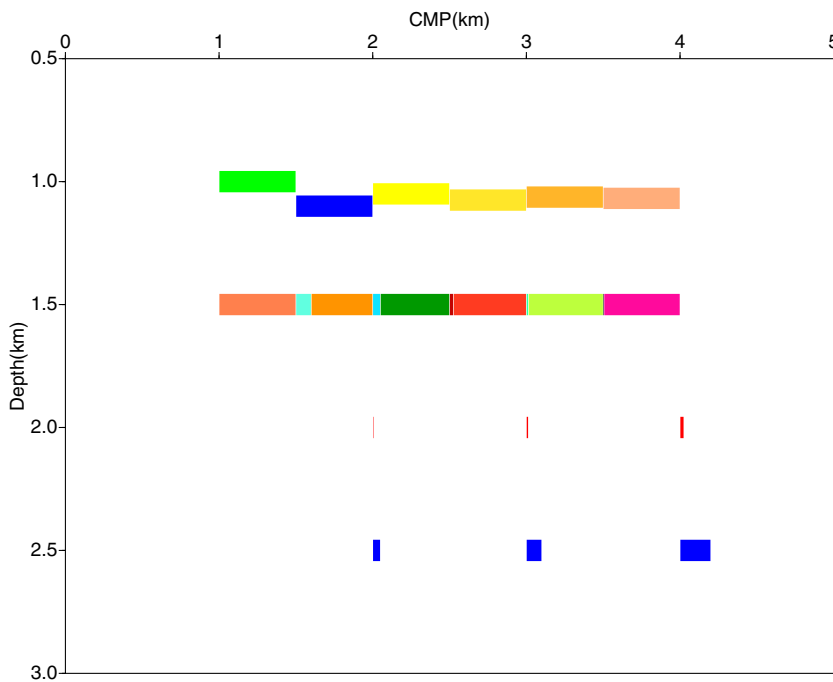


Figure 9 Multi-scale geological model.

edges remain, and the waveforms of both edges are coupled. Third, phase characteristics can be employed for the discrimination of up/down edges. For the geologies with scales from $\lambda/2$ to $\lambda/40$, the imaging features are clearly displayed. For single-edge diffractors, our dynamic diffraction imaging method returns an event with continuous polarity across the

edge. At offset-fault edges, the proposed method returns an interference of these events from both edges of the small-scale faults, which could be helpful in interpreting the displacement of the fault. For point diffractors, the proposed method returns a single event with a polarity reversal across the point. These attractive waveform properties of dynamic diffraction

Figure 10 Synthetic zero-offset section of the multi-scale geological model.

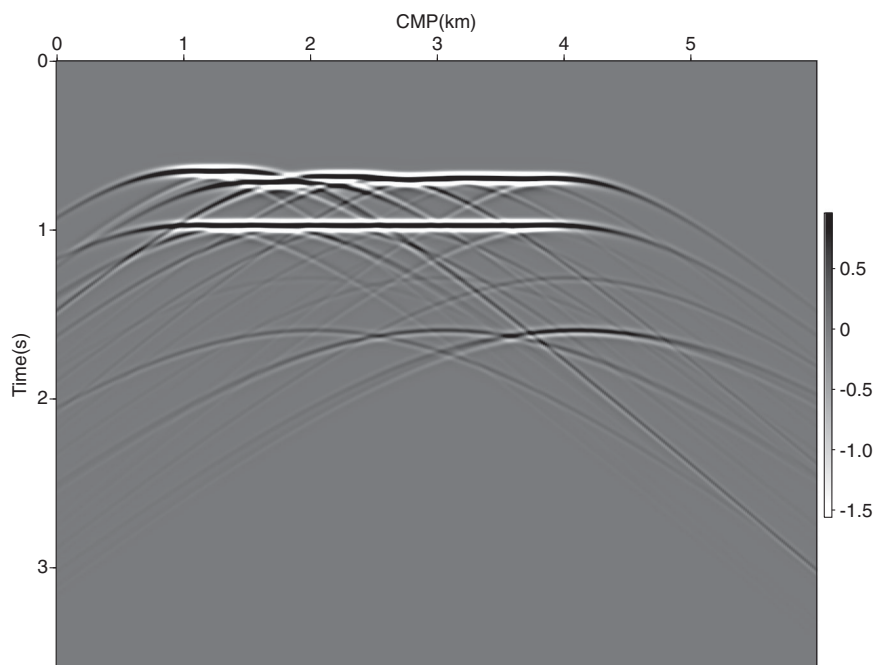
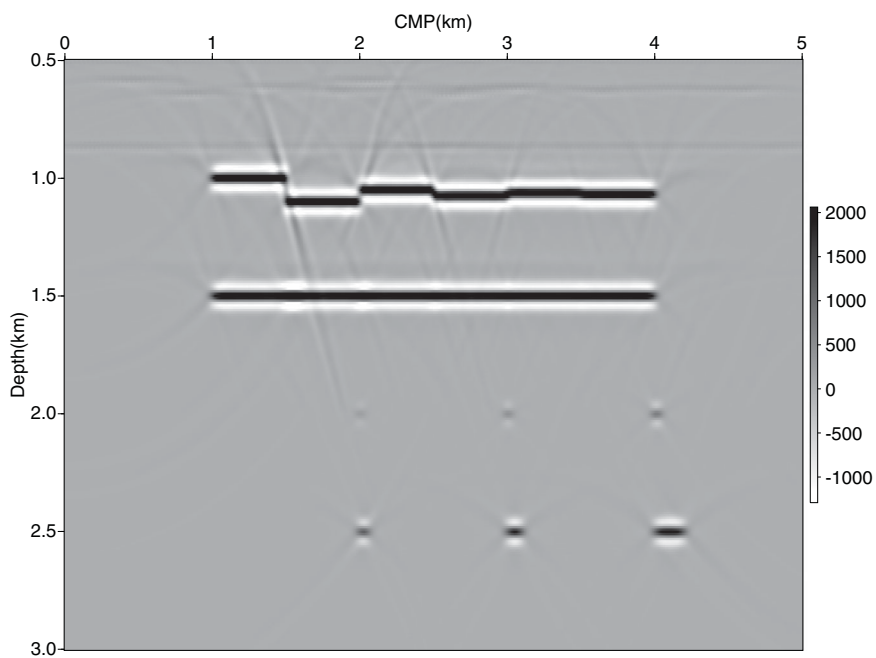


Figure 11 Conventional imaging result of the multi-scale geological model.



imaging are valuable for distinguishing small-scale faults and diffractors.

The multi-scale geological model demonstrates that removing reflection and enhancing diffraction can improve the

imaging quality of small-scale geologies, even with sizes as small as $\lambda/40$. The special features of waveforms obtained from dynamic diffraction imaging could also be used to assist in classifying the geometric shapes of geologies.

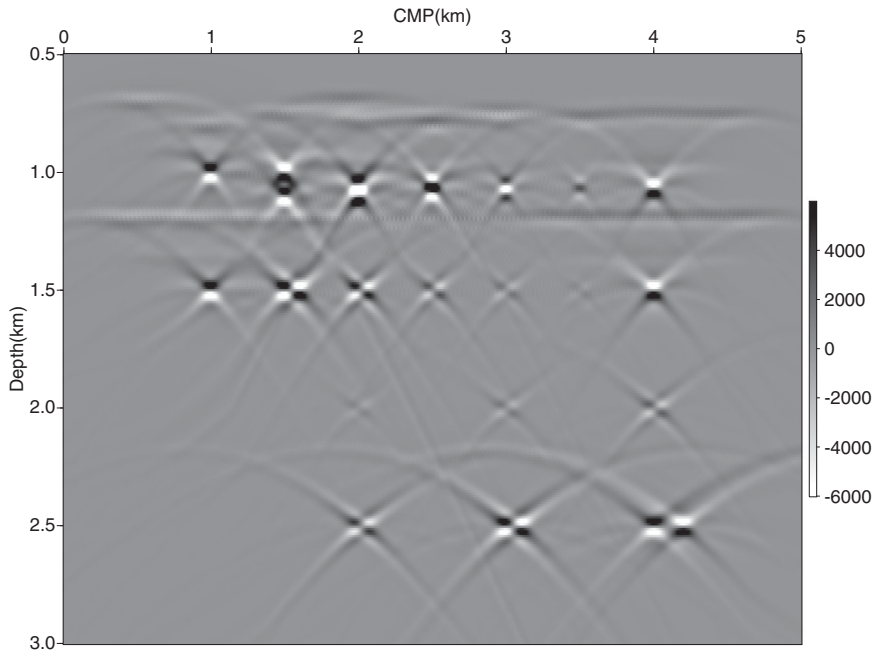


Figure 12 Dynamic diffraction imaging result of the multi-scale geological model.

3.4 2D field data example

Finally, we provide a 2D field data example to show the potential use of the proposed diffraction imaging method in high-quality reservoir imaging. Small-scale faults have strong effects on reservoir flow behaviour; hence their identification and positioning are critical in designing wells. Because identifying small-scale fractures from reflection imaging results depends on bedding displacements, we can only use the specific sizes of fractures that the seismic resolution permits. When throw decreases, geological interpretations will be unreliable. In general, the magnitudes of reflections have a strong relationship with the displacements of faults. For diffractions, their magnitudes are mainly controlled by roughness of the fault surface and by the impedance contrast between the fault zone and the surroundings.

One shot gather of the field data is displayed in Fig. 13, with the star(*) denoting the position of the source. Strong surface waves (ground rolls) and refracted waves have been eliminated. Diffracted waves are masked in the strong reflection background, with a few vague signs in the recorded seismic data.

Figure 14 illustrates the reflection imaging result, where diffractors and fractures are not well imaged. We applied the dynamic diffraction imaging scheme to shot gathers and obtained the imaging result shown in Fig. 15. As is well known, imaging results of reflections and diffractions have different

ranges of values. Thus, people generally use different gain parameters to display them. In Figs. 14 and 15, we applied the same parameters to show the imaging results. The fractures of different scales are clearly identified at several locations in the diffraction imaging section (Fig. 15). In addition, small-scale discontinuities and diffractors are enhanced in the diffraction imaging result (Fig. 15), whereas they cannot be distinguished in the reflection imaging result (Fig. 14).

The dynamic diffraction imaging method not only possesses the ability of high resolution, but also increases the signal-to-noise ratio of the imaging results to a satisfactory degree. Field data application once again verifies the validity of our proposed method.

4 DISCUSSION AND CONCLUSION

Diffraction plays a significant role in seismic data processing and interpretation. Recognition of scattering objects such as faults, pinch-outs, sharp changes in reflectivity and fractures is one of the main goals of geologists, and usually the information about them is embedded in diffraction. In essence, a reliable and physically meaningful extraction of high-resolution attributes about oil and gas reservoirs depends on the quality of diffraction imaging. Today, diffraction imaging receives much more attention because of its potential use. Geophysicists have developed

Figure 13 One shot gather of the field data example.

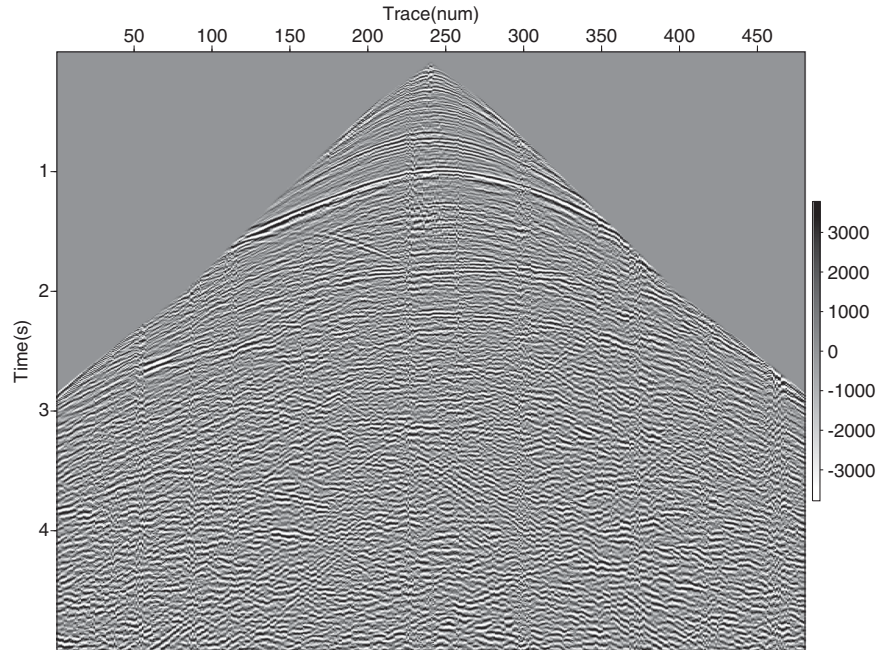
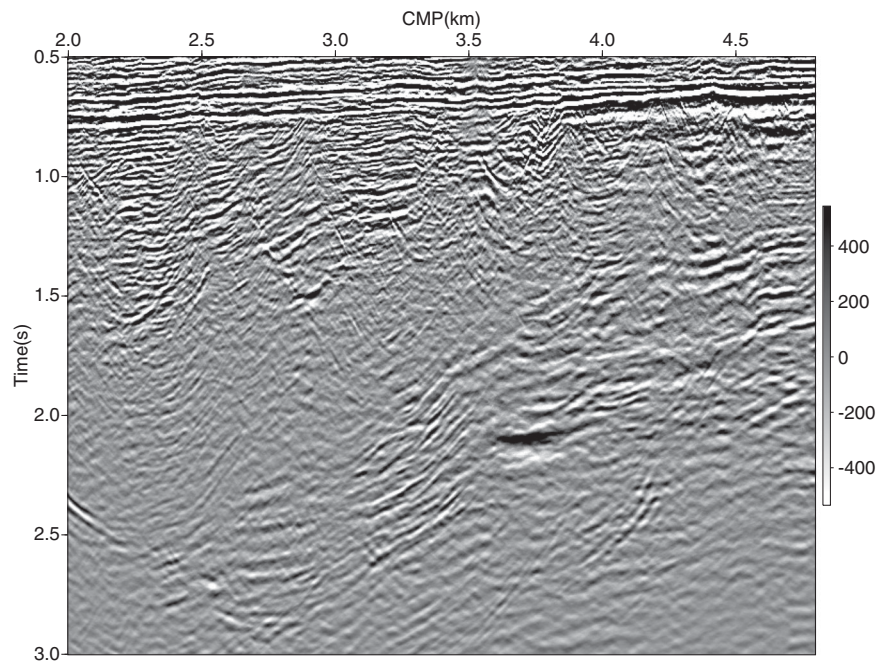


Figure 14 Conventional imaging result of the field data example with phase-reversal turned off.



many techniques to tackle the imaging problem of seismic diffractions, e.g., focusing–defocusing, plane-wave decomposition, common-reflection-surface and multi-focusing. These methods mainly focus on separating reflections and diffractions by using the distinct differences in their kinematical properties.

Based on the uniform asymptotic theory and the double exponential fitting technique, we present a dynamic diffraction imaging method to enhance edge/tip diffraction events. Conventional imaging algorithms are designed to stress reflections, where the kernels in the imaging condition are based on the stationary phase approximation. This

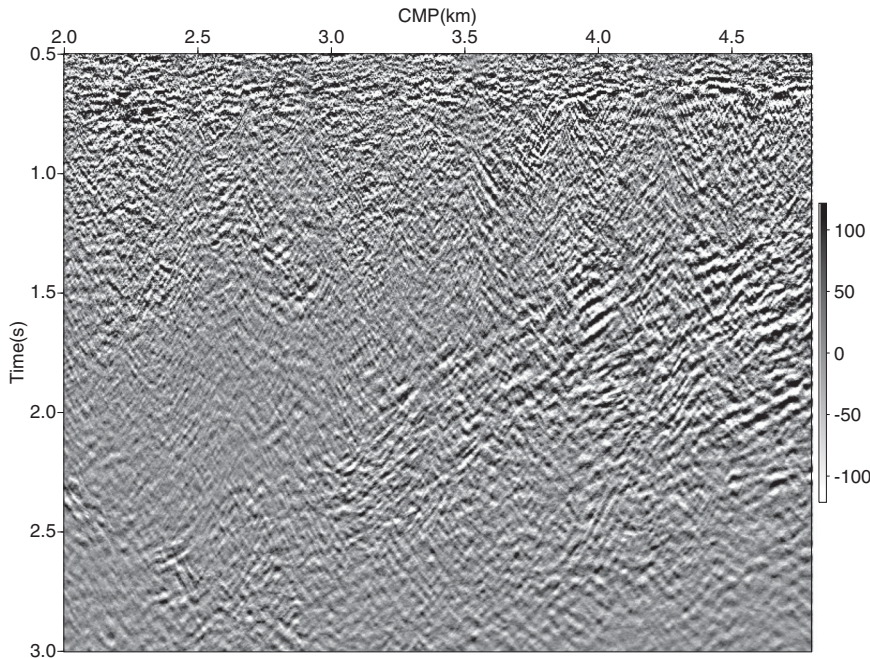


Figure 15 Dynamic diffraction imaging result of the field data example with phase-reversal turned on.

imaging principle enhances the energy within the first Fresnel zone and treats others as noises. However, the proposed diffraction imaging method performs oppositely. The uniform asymptotic diffraction theory reveals that edge/tip diffracted waves may lead to polarity reversal when they cross the primary/secondary shadow boundary, and their amplitude weakening functions take the form of a Fresnel integral. Therefore, we employed these characteristics of diffracted waves to formulate a diffraction-biased kernel to accomplish the imaging. To accelerate the calculation, a high-precision trust region algorithm is used to fit the Fresnel integral. It is well-known that diffractions are usually tangent to reflections, with their amplitudes typically lower by one or two orders of magnitude. Common kinematics-based diffraction imaging methods need to find a domain where the diffraction can be separated from the reflection. Huygens' principle illustrates that reflection events are constructed by the envelope elementary diffractions, which are tangent to reflection events at stationary points. Therefore, the proposed diffraction imaging method can remove most of the reflection and realize an automatic image of the diffraction.

In essence, diffraction is a 3D phenomenon. It illustrates transverse diffusion of energy from the shadow boundary of reflection in the direction tangential to the diffracted wavefront. The change of diffraction amplitudes can be measured with the distance from the geometrical shadow boundary and

can be calculated by using the diffraction weakening function. As long as the seismic receiver line crosses the geometrical shadow boundary, the polarity of diffracted waves will flip, and our diffraction imaging kernel will take effect. If the seismic receiver lines coincide with the shadow boundary, the diffraction energy constructed by central rays will be attenuated. This may be a limitation of the proposed method, and care should be taken during the 3D interpretation. However, because these kinds of geological structures exist in the reflection imaging results, this limitation can be overcome by combining the interpretation of the reflection and diffraction imaging results. Therefore, the proposed dynamic diffraction imaging method can be formulated as follows:

- I. If only the stationary points are found, it will be the case of a reflected wave. Continuous reflected waves with a strong energy band and stationary points will be eliminated by polarity reversal behaviour.
- II. If both the stationary points and the polarity reversal are found, it will be the case that diffractions are tangent to reflections. Hence, polarity reversal will eliminate reflection and enhance diffraction.
- III. If no stationary points and no polarity reversal are detected, it will be the case that tip/edge diffraction uncrosses the geometrical shadow boundary, or tip diffraction crosses the intersection line of even numbers of

primary shadow boundaries. In this situation, polarity reversal will be discarded and the conventional diffraction stack will be employed.

For the 3D case, the procedure of seeking stationary points will be performed along different receiver lines, or common-azimuth receiver lines. If stationary points are found, then the reflection events will be removed by polarity reversal. Hence, in our algorithm, the 3D diffraction imaging process can be treated as in the 2D situation, except for the traveltimes calculation of elementary diffraction. According to Keller's law of diffraction, a diffracted ray and its corresponding traveltimes can be determined from Fermat's principle for edge/tip diffraction. An edge/tip diffracted ray is defined to propagate along a stationary path among all the curves from source to receiver via an edge/tip point. Therefore, in the 3D diffraction imaging, a point-to-surface ray tracing algorithm should be employed to calculate diffraction traveltimes. Given a smooth velocity model, rays emitted from every imaging point to the survey surface are traced. Then an interpolation method is used to approximate traveltimes at each pair of source–receiver points.

Through investigating the dynamic characteristics of diffracted waves and the conventional Kirchhoff imaging method, we proposed a diffraction imaging method. This imaging method employs the phase and amplitude differences between diffracted and reflected waves. The algorithm is valid for small-scale geologies and for arbitrary source–receiver configurations. The proposed diffraction imaging method can increase the signal-to-noise ratio at diffraction points by the same-phase summation of diffraction energy. Moreover, the fitting weakening function behaves as an inherent window to optimize diffraction imaging apertures. These attractive characteristics mean that our proposed diffraction imaging method has an improved focusing ability.

Synthetic and field data examples illustrate the efficiency and reliability of the proposed diffraction imaging method in imaging small-scale geological bodies (such as sedimentary hiatuses, faults, unconformity interfaces and fractures). Moreover, the special phase features of diffraction imaging results can be further employed to extract information on fault edges, displacement and their relation to reflectors.

Finally, we want to point out that many issues still need to be investigated regarding the potential use of the dynamic characteristics of the diffraction imaging algorithms. In our current algorithm, there is no discrimination between edge and tip diffraction, and further work is needed to classify different types of diffractions.

ACKNOWLEDGEMENTS

We are grateful to reviewers' and the editor's very helpful comments on improvement of our paper. We are also thankful to Prof. Zuhair Nashed for his suggestions and technical discussions. This work is supported by National Natural Science Foundation of China under grant numbers 41325016 and 11271349 and R & D of Key Instruments and Technologies for Deep Resources Prospecting (the National R & D Projects for Key Scientific Instruments) under grant number ZDYZ2012-1-02-04.

REFERENCES

- Asgedom E. G., Gelius L. J. and Austeng A. 2011. A new approach to post-stack diffraction separation. EAGE, Expanded Abstracts.
- Audebert F., Nichols D., Rekdal T., Biondi B., Lumley D. E. and Urdaneta H. 1997. Imaging complex geological structure with single-arrival Kirchhoff prestack depth migration. *Geophysics* **62**(5), 1533–1543.
- Baker B. B. and Copson E. T. 1939. *The mathematical theory of Huygens' principle*. Oxford University Press.
- Bansal R. and Imhof M.G. 2005. Diffraction enhancement in prestack seismic data. *Geophysics* **70**(3), V73–V79.
- Berkovitch A., Belfer I., Hassin Y. and Landa E. 2009. Diffraction imaging by multifocusing. *Geophysics* **74**(6), WCA75–WCA81.
- Berryhill J. R. 1977. Diffraction response for nonzero separation of source and receiver. *Geophysics* **42**(6), 1158–1176.
- Burg D.W. and Verdell A.R. 2011. Depth migration of edge diffractions by adaptive weighting of migration operator amplitudes. EAGE, Expanded Abstracts.
- Clemmow P. C. 1950. A note on the diffraction of a cylindrical wave by a perfectly conducting half plane. *The Quarterly Journal of Mechanics and Applied Mathematics* **3**, 377–384.
- Clemmow P. C. 1951. A Method for the Exact Solution of a Class of Two-Dimensional Diffraction Problems. *Proceedings of the Royal Society of London. Series A, Mathematical and Physical Sciences* **205**, 286–308.
- Copson E. T. 1950. Diffraction by a plane screen. *Proceedings of the Royal Society of London* **202**, 277–284.
- Dell S. and Gajewski D. 2011. Common-reflection-surface-based workflow for diffraction imaging. *Geophysics* **76**, S187–S195.
- Deregowski S. M. and Brown S. M. 1983. A theory of acoustic diffractions applied to 2-D models. *Geophysical Prospecting* **31**, 293–333.
- Felsen L. B. 1984. Geometrical theory of diffraction, evanescent wave, complex rays and Gaussian beams. *Geophysical Journal of the Royal Astronomical Society* **79**, 77–88.
- Fomel S. 2002. Applications of plane-wave destruction filters. *Geophysics* **67**, 1946–1960.
- Fomel S., Landa E. and Taner M. T. 2006. Post-stack velocity analysis by separation and imaging of seismic diffraction. 76th SEG meeting, New Orleans, Louisiana, USA, Expanded Abstracts, 2559–2563.

- Fomel S., Landa E. and Taner M. T. 2007. Poststack velocity analysis by separation and imaging of seismic diffractions. *Geophysics* 72(6), U89–U94.
- Gelchinsky B. Ja. 1982. Scattering of waves by a quasi-thin body of arbitrary shape. *Geophysical Journal of the Royal Astronomical Society* 71(2), 425–453.
- Geoltrain S. and Brac J. 1993. Can we image complex structures with first-arrival traveltimes? *Geophysics* 58(4), 564–575.
- Goodman J. W. 1968. *Introduction to fourier optics*. McGraw-hill, New York.
- Gray S. H. and May W. P., 1994. Kirchhoff migration using eikonal equation traveltimes. *Geophysics* 59(5), 810–817.
- Hagedoorn J. G. 1954. A process of seismic reflection interpretation. *Geophysical Prospecting* 2(2), 85–127.
- Harlan W., Claerbout J. and Rocca F. 1984. Signal/noise separation and velocity estimation. *Geophysics* 49(11), 1869–1880.
- Hilterman F. J. 1970. Three-dimensional seismic modeling. *Geophysics* 35(6), 1020–1037.
- Hilterman F. J. 1975. Amplitudes of seismic waves: a quick look. *Geophysics* 40(5), 745–762.
- Kanasevich E. R. and Phadke S. M. 1988. Imaging discontinuities on seismic section. *Geophysics* 53(3), 334–345.
- Keller J. B. 1962. Geometrical theory of diffraction. *Journal of the Acoustical Society of America* 52, 116–130.
- Keller J. B. 1985. One hundred years of diffraction theory. *IEEE Transactions on Antennas and Propagation* 33(2), 123–126.
- Khaidukov V., Landa E. and Moser T. J. 2004. Diffraction imaging by focusing and defocusing: An outlook on seismic superresolution. *Geophysics* 69, 1478–1490.
- Klem-Musatov K. D. and Aizenberg A. M. 1980. The ray method and the theory of edge waves. *Geophysical Journal of the Royal Astronomical Society* 79(1), 35–50.
- Klem-Musatov K. 1994. *Theory of Seismic Diffractions*. SEG, Tulsa.
- Klem-Musatov K., Aizenberg A. M., Pajchel J. and Helle A.B. 2008. *Edge and tip diffractions theory and applications in seismic prospecting*. SEG.
- Klokov A. and Fomel S. 2012. Separation and imaging of seismic diffractions using migrated dip-angle gathers. *Geophysics* 77(6), S131–S143.
- Kozlov e., Barasky N. and Korolev E. 2004. Imaging scattering objects masked by specular reflections. SEG, Expanded Abstracts.
- Krey T. 1952. The significance of diffraction in the investigation of faults. *Geophysics* 17(4), 843–858.
- Kunz. B. F. J., 1960. Diffraction problems in fault Interpretation. *Geophysical Prospecting* 8(3), 381–388.
- Landa E. and Fomel S. 2008. Separation, imaging, and velocity analysis of seismic diffractions using migrated dip-angle gathers. SEG, Expanded Abstracts, 2176–2180.
- Landa E. and Keydar S. 1998. Seismic monitoring of diffraction images for detection of local heterogeneities. *Geophysics* 63(3), 1093–1110.
- Landa E., Shtivelman V. and Gelchinsky B. 1987. A method for detection of diffracted waves on common-offset sections. *Geophysical Prospecting* 35(4), 359–373.
- Lewis R. M. and Boersma J. 1969. Uniform asymptotic theory of edge diffraction. *Journal of Mathematical Physics* 10, 2291–2305.
- Longhurst R. S. 1973. *Geometrical and Physical Optics*. Longman, Harlow.
- Marfurt K. J., Kirlin R. L., Farmer S. L. and Bahorich M. S. 1998. 3-D seismic attributes using a semblance-based coherency algorithm. *Geophysics* 63, 1150–1165.
- Morse P. M. and Feshbach H. 1953. *Methods of Theoretical Physics*. McGraw-Hill, New York.
- Morse P. M. and Ingard K. U. 1968. *Theoretical Acoustics*. McGraw-Hill, New York.
- Moser T. J. and Howard C. B., 2008. Diffraction imaging in depth. *Geophysical Prospecting* 56(5), 627–641.
- Moser T. J. 1994. Migration using the shortest-path method. *Geophysics* 59(7), 1110–1120.
- Nichols, D. E., 1996. Maximum energy traveltimes calculated in the seismic frequency band. *Geophysics* 61(1), 253–263.
- Operto M. S., Xu S. and Lambaré G. 2000. Can we quantitatively image complex structures with rays? *Geophysics* 65(4), 1223–1238.
- Reshef M. and Landa E. 2009. Post-stack velocity analysis in the dip-angle domain using diffractions. *Geophysical Prospecting* 57(5), 811–821.
- Taner M. T., Fomel S. and Landa E. 2006. Separation and imaging of seismic diffractions using plane-wave decomposition. SEG, Expanded Abstracts, 2006–2401.
- Trorey A. W. 1970. A simple theory for seismic diffractions. *Geophysics* 35, 762–784.
- Trorey A. W. 1977. Diffraction theory for arbitrary source-receiver locations. *Geophysics* 42(6), 1177–1182.
- Tygel M., Schleicher J., Hubral P. and Hanitzsch C. 1993. Multiple weights in diffraction stack migration. *Geophysics* 59, 1820–1830.
- Wang Y. F. and Yuan Y. X. 2005. Convergence and regularity of trust region methods for nonlinear ill-posed inverse problems. *Inverse Problems* 21, 821–838.
- Wang Y. F. 2007. *Computational Methods for Inverse Problems and Their Applications* (in Chinese). Higher Education Press, Beijing.
- Zhang R. F. 2004. Fresnel aperture and diffraction prestack depth migration. CDSST annual report, 1–11.